JOURNAL OF CATALYSIS 134, 186–203 (1992)

Carbon Monoxide Hydrogenation Using Cobalt–Manganese Oxide Catalysts: The Influence of Potassium as a Promoter

SAUL E. COLLEY, MARK J. BETTS, RICHARD G. COPPERTHWAITE,*,† GRAHAM J. HUTCHINGS,‡ AND NEIL J. COVILLE*

Applied Chemistry and Chemical Technology Centre, Department of Chemistry, University of the Witwatersrand, P.O. Wits 2050, Johannesburg, South Africa

Received June 7, 1991; revised October 10, 1991

The effect of potassium promoter on the CO hydrogenation reaction over precipitated cobalt manganese oxide catalysts was studied in a plug flow laboratory microreactor (220°C, 540 kPa, GHSV = 250 h^{-1}, CO/H_2-ratio 1/1). On addition of low levels of the promoter (0.01–0.5%), significant increases in alkene/alkane ratios and higher hydrocarbon formation were observed, coupled with decreased methanation activity. Furthermore, the results showed that the presence of promoter favored the formation of longer chain alcohols, accompanied by decreases in the C_1OH–C_4OH fraction. Maximum C_5^+-hydrocarbon selectivity commensurate with high CO conversion and low methane formation was observed at between 0.1 and 0.2% potassium. C_2- and C_3-olefin selectivity was studied as a function of reactor operating conditions, and the selectivity was found to decrease with increasing temperature, pressure (constant conversion), reciprocal space velocity (space–time), and conversion. Bulk catalyst characterization by XRD and DSC suggested that the promoter did not influence the bulk structure of the catalyst. The potassium promoter concentrated on the surface as demonstrated from BET surface area measurements and XPS studies. BET measurements showed the catalyst surface area to initially decrease at low levels of promoter (0% potassium, 13.2 m^2/g; 0.01% potassium, 10.1 m^2/g), and then to increase with increased promoter loadings (1% potassium, 17.0 m^2/g). XPS studies on a 0.25% potassium promoted catalyst showed a surface aggregation of the potassium promoter from the bulk to occur during stages of calcination (6%), reduction (10%) and subsequent CO hydrogenation (2–4%). The data from the study suggest that the role of potassium is to modify the concentration of cobalt active sites and simultaneously to assist in the breakdown of the CO reactant.

It is generally accepted that the Fischer–Tropsch synthesis (CO-hydrogenation) reaction can be described as a CH_2 polymerization process which gives a broad product distribution ranging from methane to waxes (*1*). Since unsaturated hydrocarbons, especially those with two to four carbon atoms, constitute a large proportion of the feedstocks for the petrochemical industry, the maximization of yields of these lower olefins from synthesis gas using improved catalysts is of great economic interest (*2*). Moderate shifts in the broad product distributions with a specific catalyst can be obtained within the constraints of the Anderson–Schulz–Flory distribution law (*3, 4*) by variation of the reaction conditions (*5, 6*). Alternatively, the product selectivities can be modified by addition of promoters or other additives to the catalyst (*6, 7*).

The addition of small amounts of potassium to supported Group 8–10 metals (in particular iron) for Fischer–Tropsch synthesis has long been known to affect the performance of such catalysts and hence the product distribution (*6–13*). In general, po-

* To whom correspondence should be addressed.

† Present Address: Research and Development Department, AECI Ltd., P.O. Modderfontein, 1645, South Africa.

‡ Present Address: Leverhulme Centre for Innovative Catalysis, Department of Chemistry, University of Liverpool, P.O. Box 147, Liverpool L69 3BX, United Kingdom.

0021-9517/92 $3.00

tassium as a promoter has been shown to increase the olefin-to-paraffin ratio, the average molecular weight of the products, and the oxygenate content and to decrease the methanation selectivity of the catalyst.

In recent publications we have reported on the use of cobalt–manganese oxide catalysts in the Fischer–Tropsch reaction and the ability of these catalysts to enhance the C_2 and C_3 olefin content (*14–16*). In a continuation of these studies, we now report on the influence of a potassium promoter on the product composition from the CO-hydrogenation reaction. Additionally, the effect of various reaction variables (temperature, pressure, GHSV) on the product composition has also been determined. Our data are compared to the product distributions obtained on other Fischer–Tropsch promoted catalysts (*2, 6, 9, 17–20*). We also report out attempts at correlating the catalyst activity with *in situ* XRD data (reported previously (*21*)) as well as *in situ* XPS data on the catalyst.

EXPERIMENTAL SECTION

Catalyst synthesis. The synthesis of cobalt–manganese oxide catalysts used in this study has been described in detail previously (*15*). Briefly, cobalt–manganese oxide catalysts (atomic ratio Co/(Co + Mn) = 0.5) were prepared by coprecipitation from a solution of mixed metal nitrates with aqueous ammonia under controlled conditions (pH = 8.3, T = 70°C) (Maiti *et al.* (*22*)). The Co/Mn ratio in the prepared catalysts was controlled by selection of the appropriate initial mixed nitrate solution. Promotion of the precipitated and dried catalysts with potassium (as K_2CO_3) was achieved by the incipient wetness technique (*23*). Catalyst precursors were pelleted and sieved (0.5–1.0 mm particles) and then calcined in air (500°C, 24 h). Catalysts were subsequently reduced *in situ* at 400°C for 16 h in a hydrogen atmosphere (GHSV = 280 h^{-1}).

Catalyst testing. Catalyst samples (2 g) were loaded into three multi-fixed-bed laboratory reactors (*15*), which allowed the study of the CO-hydrogenation reaction over different catalysts under identical experimental conditions ($CO/H_2 \sim 1:1$ molar ratio (v/v), T = 220°C, P = 500 kPa, and GHSV = 250 h^{-1}) to be undertaken. A stabilization period of ~120 h after initiation of Fischer–Tropsch synthesis was allowed before mass-balance data collection was commenced. All catalyst activity and selectivity data were thus obtained from mass balance runs (of ~170 h), performed only after ~120 h of initial CO/H_2 reaction. No changes in the activity and selectivity of either the nonpromoted or the promoted catalysts were observed over the period of time that the different catalysts were tested. Reactions performed for up to 500 h still showed no changes in product selectivity. Product gases were analyzed by on-line gas chromatography, e.g., hydrocarbons (FID, porapak Q column) and CO, CO_2, H_2, and N_2 (TCD, carbosphere column). Condensed liquid products were analyzed using off-line gas chromatography (FID, 30 m J + W BD1 capillary column).

Catalyst characterization. X-ray diffraction measurements were carried out on a Rigaku Geigerflex D/max IIIA computer-controlled, wide-angle diffractometer at MATTEK, CSIR, Pretoria, South Africa. Surface area measurements were performed using the N_2 adsorption method with a Micromeretics Model ASAP 2000 at Sastech, Sasol 1, Sasolburg, South Africa.

XPS characterization. A 0.25% potassium-promoted cobalt–manganese oxide catalyst with a Co/(Co + Mn) bulk atomic ratio of 0.47 was prepared as described above. Calcination in air was followed by pressing a fixed mass of the catalyst powder into discs with diameters of 12.5 mm and 2 mm thickness using a standard 15-ton press. All samples were attached to a molybdenum sample holder before being loaded into the sample rod and transferred to the combined high-pressure reactor–ultrahigh-vacuum (HPR–UHV) system (*24, 25*) for treatment and analysis.

The work was carried out using an exter-

nal high-pressure reactor linked to an UHV surface analysis chamber via a sample transfer system, incorporating suitable pumping and valve arrangements. This enabled sequential reaction and surface analysis experiments to be carried out over the Fischer–Tropsch catalysts. An on-line gas chromatograph for the detection and analysis of hydrocarbon products was coupled to the reactor. The equipment used has been described previously (*24, 25*).

For all the experiments, high-purity gases were used. (Argon (99.999%), H_2 (Afrox ultrahigh-purity (UHP) 99.999%), CO (99.9%); in H_2/CO mixtures ultrahigh-purity H_2 was used along with 99.9% pure CO.) All H_2 treatments were undertaken at a temperature of 400°C and a pressure of 500 kPa.

The CO-hydrogenation studies over Co/MnO were undertaken using a temperature of 190°C and a pressure of 500 kPa. The reactions were carried out using synthesis gas with a H_2 : CO ratio of 20 : 1, along with high flow rates (approx. 500 ml min^{-1}) over the sample in order to prevent (i) excessive buildup of carbonaceous material on the catalysts, which would have made surface analysis difficult in that carbon would mask the other elements, and (ii) excessive outgassing in UHV.

During surface analysis of the cobalt–manganese oxide catalysts, significant "charging" of the sample was observed even though the sample being analyzed was electrically earthed. Such charging can be said to be due to the "p-type" semiconductor behavior of MnO (*26*), which causes an increase in electrical conductivity at high temperatures (*27*). Catalyst charging was corrected for by using an oxygen (1*s*) photoelectron signal with a binding energy (BE) of 530.0 eV as a reference (*27*). This signal remained fairly constant under all conditions, and the oxide O^{2-} was always the most abundant component at the surface.

Computer fitting of up to three Gaussian peaks to the raw data using a modified commercially available least-squares fitting routine facilitated the determination of peak areas and subsequent quantification of the XPS data (*25*). Quantification of our XPS data on the compressed Co/Mn discs gave an accuracy of ±5%.

Calculation of photoelectron escape depths for these catalysts is further complicated by the segregation of various components in the solid during treatments. This results in compositional changes, including density changes that could not be measured using our equipment.

Surface concentration values "η" for an element were obtained from the equation (*28*)

$$\eta = \frac{ASE_k}{\sigma\lambda_\tau(E_k)},$$

where A is the integrated XPS signal area, S is the detector sensitivity setting for an element, σ is the photoionization probability, and λ_τ is the mean free path of photoelectrons with energy E_k (*25*) (see Appendix for further details).

Approximate values for the total surface concentrations were obtained by adding the η values of detected elements, $\eta_{total} = \eta_1 + \eta_2 + \eta_3 + \ldots + \eta_i$.

The relative surface atomic percentage (r.s.a.p.) of each element (for example, element 1) was calculated using the following equation:

$$\text{r.s.a.p.}_1 = \frac{\eta_1}{\eta_{total}} 100\%.$$

The 0.25% potassium-promoted cobalt–manganese oxide catalyst was studied both under reducing and under CO-hydrogenation conditions. The catalyst was analyzed by XPS in the following sequence: before treatment, after 12 h H_2 reduction (400°C), after 15 min Fischer–Tropsch synthesis, after 1 h Fischer–Tropsch synthesis, after 3 h Fischer–Tropsch synthesis, after 6 h Fischer–Tropsch Synthesis, after 12 h Fischer–Tropsch synthesis, after 12 h H_2 reduction (400°C) and after Ar^+ bombardment (5 kV beam energy for 5 min). The

TABLE 1

Selectivities of CO-Hydrogenation Using K-Promoted Co/MnO Catalysts[a]

% K promotion	0.0	0.01	0.05	0.1	0.25	0.5	1.0
Reaction time/h	170	103	170	144	170	144	144
GHSV/h^{-1}	268	236	253	254	267	251	251
CO conversion (%)	44.1	43.0	38.8	39.0	37.5	28.7	21.1
α^b	0.79	0.84	0.84	0.86	0.86	0.85	—
			Hydrocarbon selectivity (% m/m)				
CH_4	8.3	6.9	5.8	4.2	4.7	6.0	14.5
C_2H_4	2.3	2.3	2.7	1.9	2.7	3.1	8.3
C_2H_6	3.5	3.0	1.4	1.4	0.6	0.6	1.5
C_3H_6	13.6	13.8	12.2	10.1	9.9	8.6	15.3
C_3H_8	3.7	3.4	2.7	2.2	1.8	1.8	3.4
C_4	9.3	9.3	9.5	7.4	7.9	7.7	13.1
C_5^+	38.2	39.3	40.1	47.2	47.8	48.5	36.9
Total C_3 hydrocarbon	17.3	17.2	14.9	12.3	11.7	10.4	18.7
C_2–C_4 fraction	32.4	31.6	28.5	23.0	21.9	21.8	41.8
			Alcohol selectivity (% m/m)				
CH_3OH	0.6	0.5	0.6	0.6	0.3	0.2	—
C_2H_5OH	2.0	1.8	1.3	1.4	0.8	0.4	—
1-C_3H_7OH	3.9	3.7	3.6	3.5	3.8	2.0	—
1-C_4H_9OH	1.0	1.4	1.7	1.6	1.3	0.9	—
C_5OH^+	8.3	9.1	11.9	11.5	14.1	16.6	—

[a] Pressure 540 ± 40 kPa and temperature 220°C.
[b] Anderson–Schulz–Flory chain growth probability factor.

hydrocarbon selectivity data after Fischer–Tropsch synthesis are shown in Table 5 below.

RESULTS AND DISCUSSION

The effects of potassium loading on the performance of Co/MnO catalysts during the hydrogenation of carbon monoxide are presented in Table 1. The addition of small amounts of potassium was shown to affect the performance of such catalysts in a variety of ways, viz., catalyst activity, methane and heavy hydrocarbon selectivity, olefin to paraffin ratios, and primary alcohol selectivities. Each of these effects will be discussed separately below.

Although the Co/MnO catalysts showed an almost immediate hydrocarbon synthesis activity (~25% CO conversion after only 1 h time on stream), the catalyst still required a stabilization or "bedding-in" period of ~120 h (T = 220°C, P = 500 kPa, and GHSV ~250 h^{-1}) for maximum stable activity and selectivity to be attained. During this period the activity increased to ~43% CO conversion, which was also accompanied by a decrease in methane selectivity and a corresponding increase in both the C_2 and C_3 selectivity, as shown in Fig. 1. It was observed that the duration of this stabilization period was not altered by the amount of the potassium promoter added (0–1% potassium).

The effect of potassium loading on *catalyst activity* is shown in Table 1 and Fig. 2. The data indicate that only low levels (between 0.01 and 0.25%) of potassium were required to produce decreased methane and increased olefin selectivities. This was, however, accompanied by a decrease in catalytic activity, viz., a 6% activity decrease was observed for a potassium loading of between 0.1 and 0.2% when compared to the unpromoted catalyst. A significant decline in activity resulted from the addition of higher levels of potassium with the 1.0%

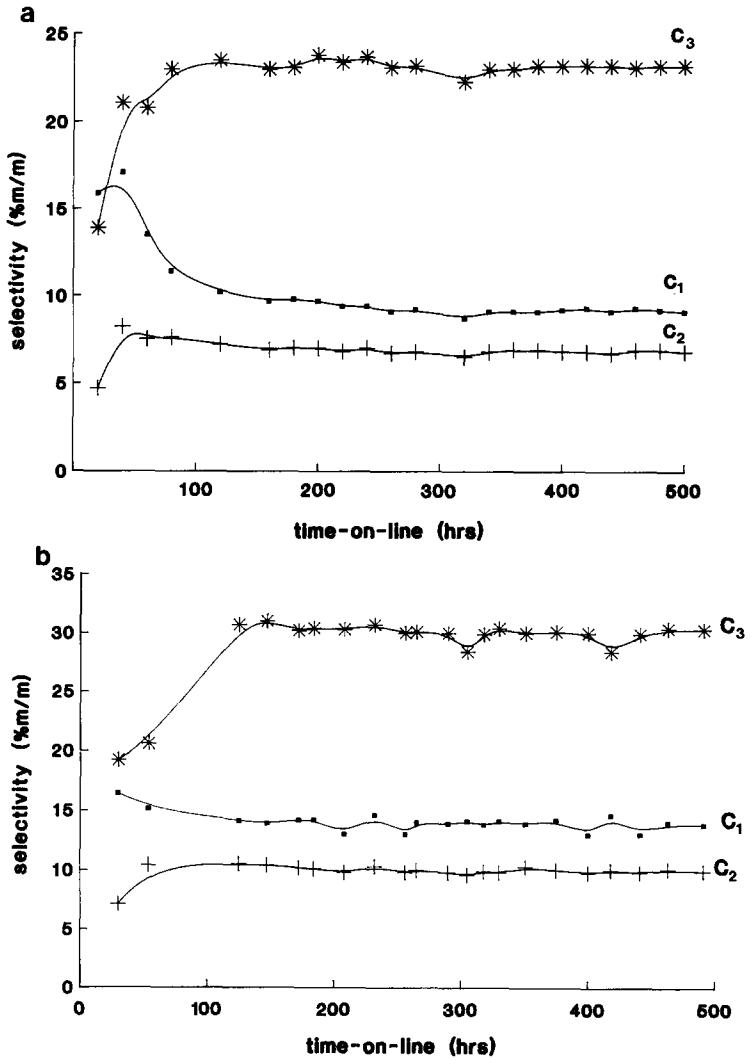

FIG. 1. C_1, C_2, and C_3 selectivities versus time on stream, showing the stabilization period for the Co/MnO catalyst with (a) 0.0% K and (b) 0.25% K. The data used in these plots do not reflect selectivities from complete mass balance calculations, but rather % m/m selectivities from the gaseous fraction alone.

potassium promoted catalyst exhibiting a CO conversion reduced to half that of the unpromoted system. The low levels of alkali used for optimum catalytic performance of the Co/MnO catalysts are consistent with the alkali loadings used for the promotion of similar catalysts (*29, 30*). The variations in weight fractions for the carbon number ranges C_1, C_2–C_4 and C_{5+} show that the decrease in methane selectivity coupled with a corresponding decrease in the C_2–C_4 fraction, see Table 1, was accompanied by an increase of the high molecular weight fraction (C_{5+} formation) on addition of the potassium promoter.

The observed shift to higher molecular weight hydrocarbons with potassium promotion was substantiated by an increased chain growth probability factor α, calculated from the Anderson–Schulz–Flory

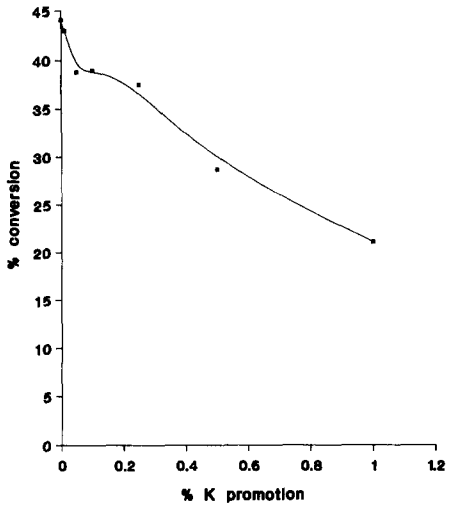

FIG. 2. Influence of % potassium content on CO conversion.

plots for a set of potassium–metal addition catalysts (Table 1).

Potassium-promoted catalysts showed enhanced olefin selectivities for the C_2 and C_3 fractions, with the optimum potassium loading again being between 0.1 and 0.2% potassium. Although an overall decrease in the selectivities for total C_2 and C_3 hydrocarbons was observed, the addition of promoter generated an increasing percentage of olefins in these C_2 and C_3 light gas fractions.

Primary alcohol selectivities are given in Table 1, with $C_1OH \rightarrow C_4OH$ and C_5OH^+ fractions being plotted as a function of potassium loading, and presented in Fig. 3. These results showed that the presence of potassium favored the formation of longer chain alcohols accompanied by decreases in $C_1OH \rightarrow C_4OH$ selectivities. These trends held true for potassium loadings of up to ~0.5%.

Effect of Operating Conditions on the Alkene/Alkane Ratios

Typical hydrocarbon product distributions for 0.0 and 0.25% potassium-promoted Co/MnO catalysts at three different operating temperatures of 190, 220, and 250°C are shown in Table 2 (at fixed pressure and space velocity of 500 kPa and 280 h^{-1}, respectively). On increasing the temperature, methane selectivity increased significantly and it became a major hydrocarbon product at the expense of the higher hydrocarbons. As the temperatures decreased, the olefin to paraffin ratios for the C_2 and C_3 fractions increased dramatically for both the promoted and nonpromoted catalysts. Therefore it appears that at high temperatures secondary hydrogenation of the primary alkenes is favored.

The space velocity was varied by changing the gas flow rate for a given mass of catalyst at a fixed pressure (500 kPa) and temperature (220°C). Figure 4 shows a plot of C_2 and C_3 olefin to paraffin ratios as a function of inverse space velocity (space–time) for a series of 0.0, 0.1, and 0.25% potassium-promoted Co/MnO catalysts. Slight decreases in the alkene/alkane ratios were observed in changing the inverse space velocity from 1.7×10^{-3} to 6.7×10^{-3} h (i.e., gas hourly space velocity from 600 to 150 h^{-1}). The C_2 fractions appear to be more sensitive to change in inverse space velocity than their C_3 counterparts, with a greater decrease in the C_2 olefinity being observed with increasing inverse space ve-

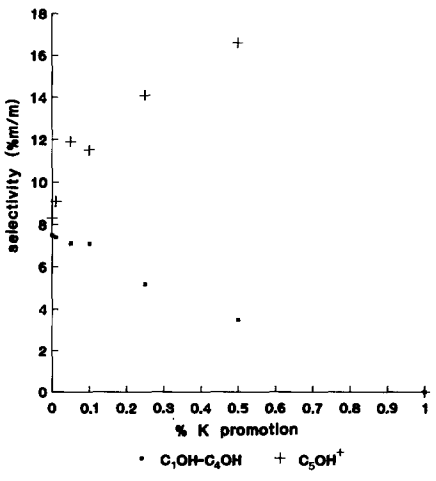

FIG. 3. C_1OH–C_4OH and C_5OH^+ alcohol fractions as a function of potassium promoter.

TABLE 2

Hydrocarbon Distribution at Different Temperatures for Promoted and Unpromoted Co/MnO Catalysts[a]

T/°C	0.0% K			0.25% K		
	190	220	250	190	220	250
% CO conversion	17.3	44.1	56.4	13.8	37.5	45.9
	Product Selectivities/% m/m					
C_1	6.9	8.3	16.7	4.3	4.7	12.9
$C_2{=}/C_2{-}$	1.0	0.7	0.3	7.8	4.5	2.7
$C_3{=}/C_3{-}$	4.9	3.7	2.0	8.0	5.5	3.2
C_4	11.1	9.3	9.7	9.4	7.9	6.3
C_{5+}	43.5	38.2	29.4	41.5	47.8	36.9
Total oxygenates	tr	15.8	11.5	tr	20.3	15.9

[a] P = 500 kPa, GHSV = 280 h^{-1}.

locity. This is consistent with earlier observations that ethene was the more reactive of the olefins (*18*), and would consequently be more susceptible to any change that increased the hydrogenating properties of the system.

These decreases in olefinity are a result of increased contact times, which would consequently increase the probability of secondary hydrogenation of the primary alkenes. Similar trends of decreasing olefin-to-paraffin ratios with increasing space–time on an iron catalyst was also found by Bussemeier *et al.* (*2*); i.e., the primary products of reaction are the α-olefins which are hydrogenated to corresponding paraffins. Arakawa and Bell (*17*), also on iron catalysts, have shown the olefin-to-paraffin ratio to increase with increasing flow rate, again indicating that olefins are primary synthesis products, and that a substantial portion of C_{2+} paraffins is formed by hydrogenation of the olefins.

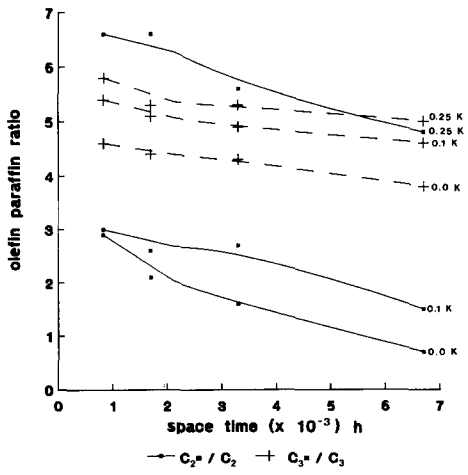

FIG. 4. Effect of inverse space velocity on the C_2 and C_3 alkene/alkane ratios ($P \approx 500$ kPa, $T \approx 220$°C).

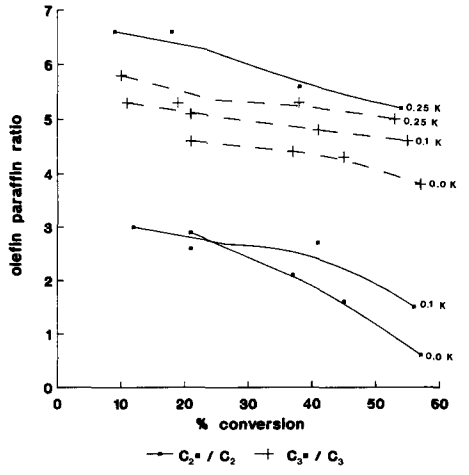

FIG. 5. Effect of conversion on the C_2 and C_3 alkene/alkane ratios ($P \approx 500$ kPa, $T \approx 220$°C).

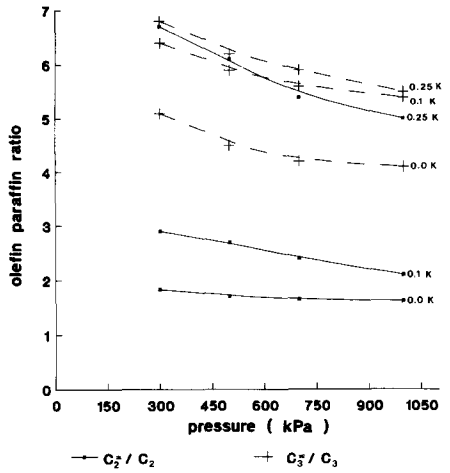

FIG. 6. Effect of pressure (at *constant contact time*) on alkene/alkane ratios for the C_2 and C_3 hydrocarbon fractions ($T \approx 220$°C).

TABLE 3

Influence of the K Promoter on the BET Surface Areas[a]

% K promoter	BET surface area ($m^2\ g^{-1}$)[b]
0.0	15.7
0.0 (treated with H_2)	13.2
0.01	10.1
0.05	11.1
0.1	11.9
0.25	14.2
0.5	16.6
1.0	17.0

[a] Outgassing temperature 150–170°C, outgassing time 16–18 h, outgassing pressure 5×10^{-6} mbar, adsorption temp. 76°K (liquid nitrogen, adsorption gas = N_2).

[b] The surface areas were corrected for the physical influence of H_2O (as used in the promotion procedure), reflecting the change in surface areas due to the influence of K promoter alone.

It is difficult to isolate the effect of inverse space velocity, since inevitably conversion increases with increasing inverse space velocity. Thus a plot of C_2 and C_3 olefin-to-paraffin ratios as a function of varying conversions for the same series of catalysts is given in Fig. 5. Similar trends were observed with increased CO conversions, with the C_2 fraction again being more sensitive to change than its C_3 counterpart. The above results are consistent with work done on unpromoted Fe/MnO and Co/MnO catalysts (*15*), MnO-supported cobalt and nickel catalysts (*19*), and potassium-promoted cobalt and iron carbonyl cluster-derived catalysts (*31*).

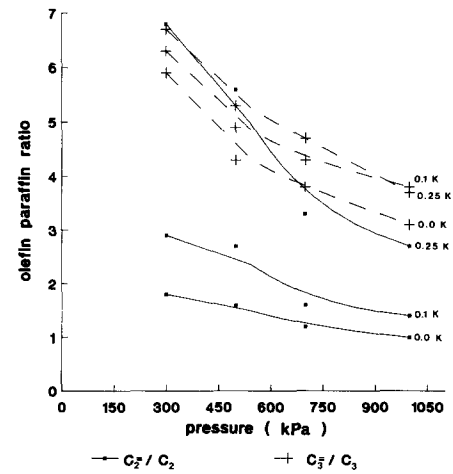

FIG. 7. Effect of pressure (at *variable contact time*) on the C_2 and C_3 alkene/alkane ratios ($P \approx 500$ kPa, $T \approx 220$°C).

CO-hydrogenation reactions were also performed on the same series of cobalt catalysts at three different pressures, 300, 500, and 1000 kPa ($T \approx 220$°C). For comparative purposes the pressures were varied at a *constant contact time*; i.e., since contact time is proportional to pressure but inversely proportional to GHSV, a constant contact time was maintained by compensating increasing pressure with increasing gas hourly space velocity. The effect of pressure on the alkene/alkane ratios is shown in Fig. 6, which demonstrates that on increasing pressure, slight decreases in alkene selectivity for both the C_2 and C_3 hydrocarbons had occurred.

Further investigations of the influence of pressure on alkene selectivity were performed by changing pressure at a *constant GHSV*, i.e., *variable contact time*, rather

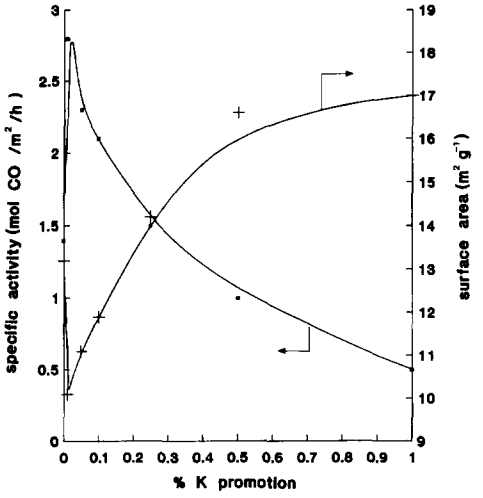

FIG. 8. Surface areas and corresponding specific activity versus potassium promotion.

than a constant contact time, as previously. Since contact time is related to pressure, increasing the pressure from 300 to 1000 kPa would have the effect of increasing the contact time more than threefold. The results of increasing pressure (at GHSV $\approx 250\ h^{-1}$) on C_2 and C_3 alkene/alkane ratios are given in Fig. 7.

These results show that on increasing pressure (with increasing contact time) a marked decrease in olefinity of the products occurred, when compared to only slight decreases in olefinity observed for increasing pressure at a constant contact time—cf. Fig. 6.

Bulk and Surface Characterization

Structural changes of coprecipitated Co/MnO catalysts during calcination, reduction, and Fischer–Tropsch synthesis have been reported (*21*). In summary, the calcined catalyst precursors were found to consist of mixed Co–Mn oxide spinels identified as $(Co,Mn)(Co,Mn)_2O_4$ and $CoMnO_3$, which were subsequently reduced to a solid solution of Co(fcc) + MnO. After an extended period of synthesis (~120 h), the Co(fcc) had transformed into a body centered cubic form [Co(bcc)], which is believed to be its "true" active phase for CO hydrogenation (*32*).

Although *in situ* investigations of the potassium-promoted cobalt catalysts were not performed, *ex situ* XRD studies performed on a series of potassium-promoted (0.0–1.0% potassium) calcined (500°C, in air) Co/MnO catalysts suggested that the incorporation of the alkali did not in any way affect the bulk structure of the catalysts. This was confirmed by a DSC characterization, performed on the same series of catalysts, during their calcination in air (temperature ramp 25 → 550°C at 5°C min^{-1}). If absent from the bulk, the potassium promoter would then essentially occupy the catalyst surface, and would consequently influence the surface composition and topology of the catalyst; the promoter would not be de-

TABLE 4

Relative Surface Atomic Percentages of Elements between Various Treatments[a] for the CO-Hydrogenation Study with K-promoted Co/MnO Catalysts

Catalyst Loading	r.s.a.p.'s of elements for various loadings				
	C	O	Mn	Co	K
1	18.1	56.3	13.2	5.9	6.0
2	5.1	60.1	19.6	4.4	10.0
3	7.9	60.4	18.9	6.6	6.2
4	12.7	59.3	19.1	7.2	1.7
5	6.2	63.1	20.9	7.7	2.1
6	28.6	49.1	16.4	5.9	trace
7	32.3	42.8	15.6	5.0	4.5
8	7.9	57.4	19.5	6.3	8.9
9	trace	63.6	27.2	9.2	8.0

[a] R.s.a.p.'s were determined (1) before treatment; (2) after 12 h H_2 (400°C); (3) after 15 min Fischer–Tropsch synthesis; (4) after 1 h Fischer–Tropsch synthesis; (5) after 3 h Fischer–Tropsch synthesis; (6) after 6 h Fischer–Tropsch synthesis; (7) after 12 h Fischer–Tropsch synthesis; (8) after 12 h H_2 (400°C); (9) after Ar^+ bombardment (5 kV beam energy for 5 min).

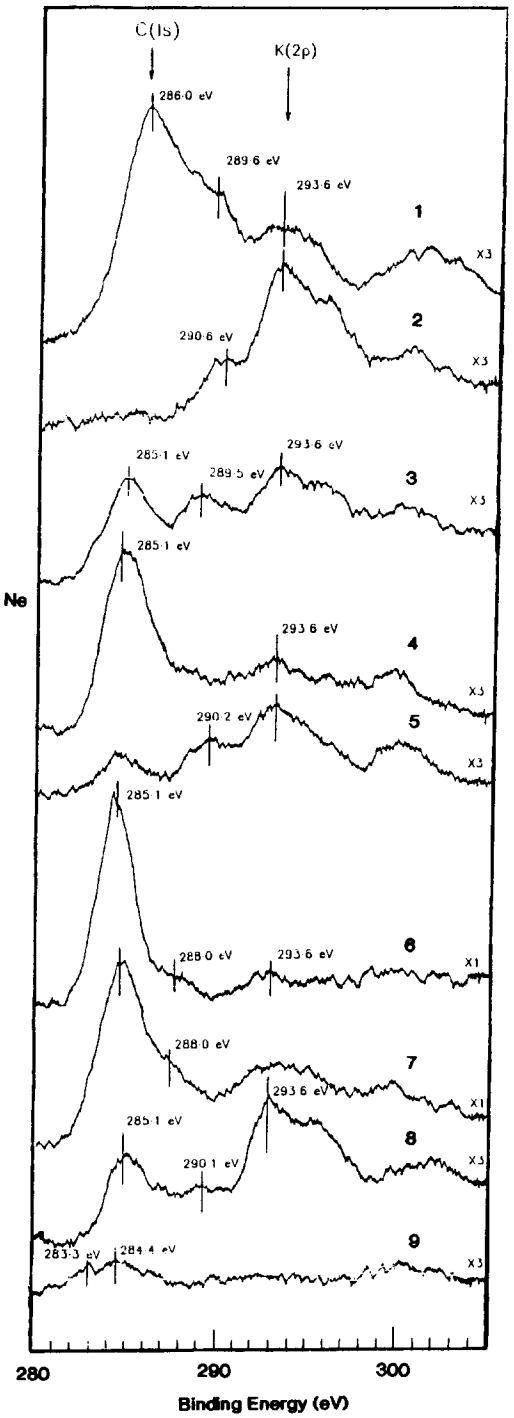

FIG. 9. XPS spectra recorded in the C (1*s*) and K (2*p*) regions between various treatments for the CO hydrogenation study with potassium promoted Co/MnO. Spectra were recorded: (1) before treatment; (2) after 12 h H_2 (400°C); (3) after 15 min Fischer–Tropsch synthesis; (4) after 1 h Fischer–Tropsch synthesis; (5) after 3 h Fischer–Tropsch synthesis; (6) after 6 h Fischer–Tropsch synthesis; (7) after 12 h Fischer–Tropsch synthesis; (8) after 12 h H_2 (400°C); (9) after Ar^+ bombardment (5 kV beam energy for 5 min).

tected from bulk XRD and DSC characterization.

Therefore these changes were monitored by surface-sensitive techniques on a 0.25% potassium-promoted Co/MnO catalyst. The BET surface areas of a series of calcined (500°C, 24 h) alkali-impregnated catalysts are given in Table 3. The BET data show clearly that potassium influences the surface areas. The surface area decreased initially with increasing alkali content, and then increased and eventually exceeded that of the unpromoted catalyst. These results are consistent with those of Dry and Oosthuizen (*10*), who showed that the alkali promoter decreased the surface areas of reduced iron catalysts, and that a greater loss in areas was recorded the more basic the alkali added (alkali promotions were on the order of 0–2.0 g/100 g iron).

The surface areas, with corresponding specific activities for the potassium-promoted series, are illustrated in Fig. 8. This shows the specific activity to initially increase with increasing potassium content (with corresponding decreases in surface area), and then to decrease (with corresponding increases in the surface area). Although the overall CO conversion has been shown to decrease with increasing potassium content (see above), the *specific activity* increases initially and then starts to decline rapidly with increasing promoter content. This specific activity decrease is more rapid than the increase in the surface area (Fig. 8). This is a particularly significant observation since it indicates that on an active surface basis, addition of K^+ does promote both activity and selectivity.

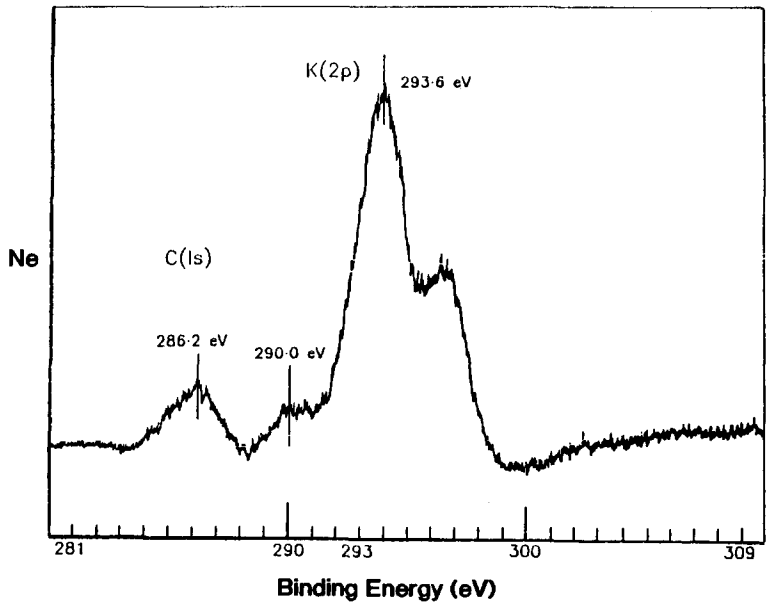

FIG. 10. XPS spectrum recorded in the C (1*s*) and K (2*p*) regions of pure, untreated K_2CO_3.

XPS Studies

The promoted catalyst was also analyzed by XPS in the sequence calcination, reduction, Fischer–Tropsch synthesis, re-reduction, and finally Ar^+ bombardment. Table 4 summarizes changes in surface composition during these treatments.

Before treatment, the carbon (1*s*) peak had a pronounced shoulder with a BE of 289.6 eV (see Fig. 9). This is assigned to a CO_2(ad) species as well as surface carbonate from K_2CO_3. (Thermogravimetric analysis of samples of pure K_2CO_3 in both ambient (oxidizing) and hydrogen atmospheres has shown that K_2CO_3 is thermally stable up to 850°C) (*33*). We are unable to assign the main carbon (1*s*) signal with a BE of 286.0 eV, which, however, plays no part in the catalytic reactions which follow.

The r.s.a.p. of potassium of 6%, compared with a bulk concentration of 0.25%, is indicative that calcining the catalysts causes segregation of potassium to the surface. The potassium (2*p*) signal at a BE of 293.6 eV is broad and does not have a clear doublet structure, as do K_2O and KOH or pure potassium as studied on metallic cobalt by Bonzel and co-workers (*34*). Carbon (1*s*) and potassium (2*p*) spectra of pure, untreated K_2CO_3 show that the potassium (2*p*) peak is in the form of a 2 : 1 doublet and there is a carbon (1*s*) signal at 290.0 eV (presumably from CO_3^{2-}) (see Fig. 10).

Prior to treatments, the Co/Mn surface atomic ratio is 0.45. The manganese ($2p_{3/2}$) signal has a maximum at 640 eV, and there is no clear evidence of a shake-up satellite, which is possibly obscured through peak broadening (Fig. 11). The observed shape of the peak may also be explained by the presence of Mn_3O_4 coupled to the presence of alkali promoter at the surface. The surface manganese of the calcined catalyst is not as oxidized as pure Co/MnO samples (*35*), indicating that CO_3^{2-} ions may be in lattice sites previously occupied by excess O^{2-} ions, with K^+ being in the cation vacancies.

The cobalt ($2p_{3/2}$) signal is clearly due to Co^{2+} as indicated by the BE of the peak at 780.3 eV and the shake-up satellite associated with a high-spin (d^7) configuration (Fig. 12).

The oxygen (1*s*) signal is asymmetric (Fig.

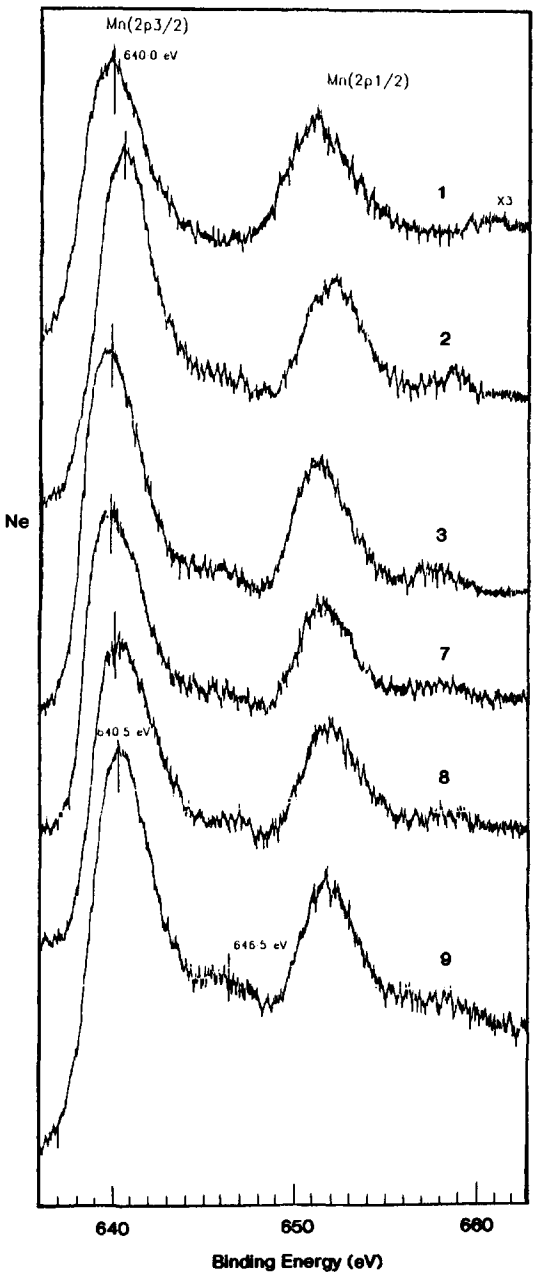

FIG. 11. XPS spectra recorded in the Mn ($2p_{3/2}$) and Mn ($2p_{1/2}$) region at higher sensitivity for the CO-hydrogenation study with potassium promoted Co/MnO. Spectra were recorded: (1) before treatment; (2) after 12 h H_2 (400°C); (3) after 15 min Fischer–Tropsch synthesis; (7) after 12 h Fischer–Tropsch synthesis; (8) after 12 h H_2 (400°C); (9) after Ar^+ bombardment (5 kV beam energy for 5 min).

13). The r.s.a.p.'s of oxygen and potassium are 56.8 and 6% respectively. If all the potassium is in the form of K_2CO_3, 16% of the oxygen (1*s*) signal is caused by the high BE shoulder. Since curve fitting shows that a larger portion than 16% constitutes the high BE shoulder on the oxygen (1*s*) signal, the extra intensity is probably due to oxygen from CO_2(ads) species.

Reduction with hydrogen for 12 h has the effect of removing all carbon with a BE of 286.0 eV, but there is still carbon present with a BE of 290.6 eV. A carbon (1*s*) BE of around 290 eV can be associated with an adsorbed CO_2 species (which are known to desorb with increased temperature), and can be taken as evidence that the peak at 290.6 eV is now associated with the carbonate of the K_2CO_3 promoter. The r.s.a.p.'s of carbon (5.1%) and potassium (10.1%) indicate that most, if not all of the potassium is in the form of K_2CO_3 after reduction. This finding is in contrast to evidence reported by Benzel *et al.* who suggest the presence of KOH after reduction of KNO_2-, K_2CO_3-, and KOH-promoted iron and platinum surfaces (*36*), but using different experimental conditions.

The r.s.a.p. of potassium after reduction increases from 6.1 to 10.1% and is associated with a change in shape of the potassium (2*p*) XPS signal which is seen to more closely approach that of a clear 2 : 1 doublet. The promoter has thus segregated to the surface. This is consistent with other studies that have observed surface mobility of potassium promoters (*25, 37*).

Treatment with H_2 has the effect of lowering the Co/MnO ratio from 0.45 to 0.25. After reduction the manganese ($2p_{3/2}$) signal becomes narrower and a shake-up satellite becomes more evident. The H_2 treatment therefore gives rise to MnO. Reduction of the surface cobalt is incomplete, as shown by the broader cobalt ($2p_{3/2}$) signal with the metallic and oxide components. The presence of Co^{2+} is confirmed by the shake-up satellite, which is still present (albeit suppressed). This suggests that metallic cobalt

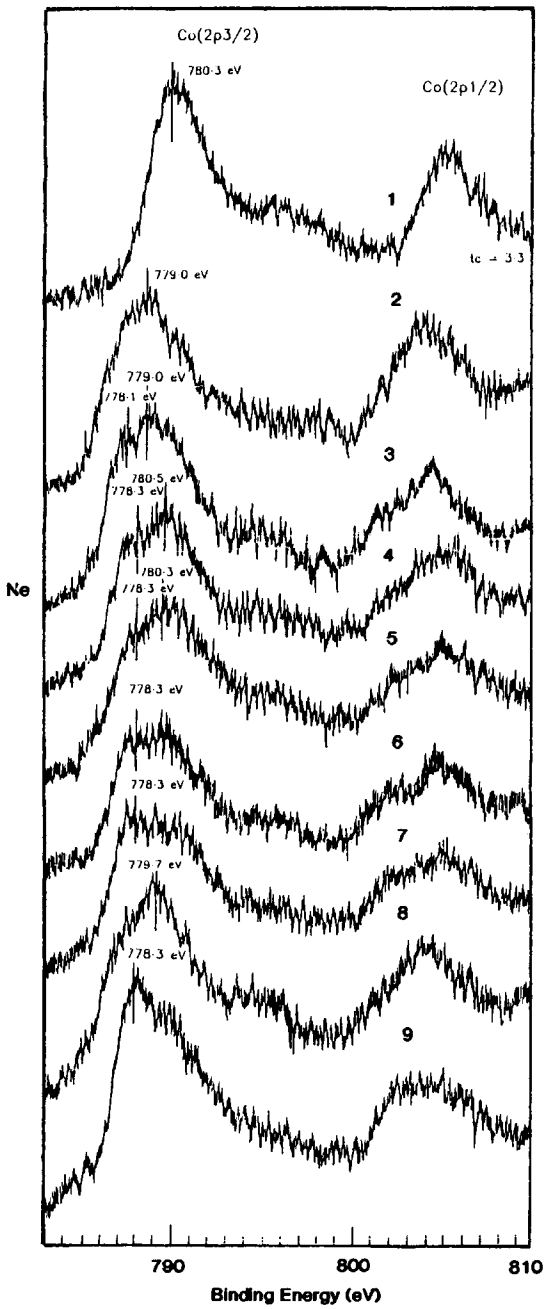

FIG. 12. XPS spectra recorded in the Co ($2p_{3/2}$) and Co ($2p_{1/2}$) region between various treatments for the CO hydrogenation study with potassium promoted Co/MnO. Spectra were recorded: (1) before treatment; (2) after 12 h H_2 (400°C); (3) after 15 min Fischer–Tropsch synthesis; (4) after 1 h Fischer–Tropsch synthesis; (5) after 3 h Fischer–Tropsch synthesis; (6) after 6 h Fischer–Tropsch synthesis; (7) after 12 h Fischer–Tropsch synthesis; (8) after 12 h H_2 (400°C); (9) after Ar^+ bombardment (5 kV beam energy for 5 min).

may be mobile, and that reduction may start in the bulk. This suggestion, as well as the observation of incompletely reduced cobalt at the surface, may explain the lowered Co/Mn ratio after reduction. Obviously potassium inhibits reduction of the catalyst surface and this is clearly shown by the behavior of the cobalt. The presence of K_2CO_3 would lower the number of cation vacancies in the MnO lattice, resulting in metallic cobalt with reduced diffusion capability.

After 15 min of Fischer–Tropsch synthesis over the potassium-promoted Co/MnO catalyst, carbon with a BE of 285.1 eV is seen to appear and this is once again assigned to a hydrogenated carbon species. The peak with a BE of 289.5 eV is seen to increase relative to the potassium ($2p$) signal which retains its doublet shape. There is no evidence for graphitic or carbidic carbon after exposure to synthesis gas.

The GC trace recorded at 15 min of Fischer–Tropsch synthesis indicates that the potassium has a profound effect on the hydrocarbon distribution when compared to a GC spectrum taken at the same time (with the same reaction conditions employed) but using unpromoted Co/MnO (Table 5). Potassium has the effect of lowering methane production, increasing the olefin to paraffin ratio, and increasing the average hydrocarbon chain-length. These findings correspond well to the bulk reactor studies performed with these catalysts.

XPS spectra were recorded on the catalyst after 1, 3, 6, and 12 h of Fischer–Tropsch synthesis. After 6 and 12 h of Fischer–Tropsch synthesis, the hydrogenated carbon species is seen to increase and the r.s.a.p.'s of carbon are 28.6 and 32.3% respectively. There is also evidence suggesting a carbon species with a carbon ($1s$) BE of 288.0 eV, and this may be due to an oxygenated hydrocarbon or CO(ads) species. This may explain the higher oxygenated hydrocarbon production observed during CO-hydrogenation over potassium-promoted Co/MnO in these studies.

The manganese ($2p_{3/2}$) signal remains

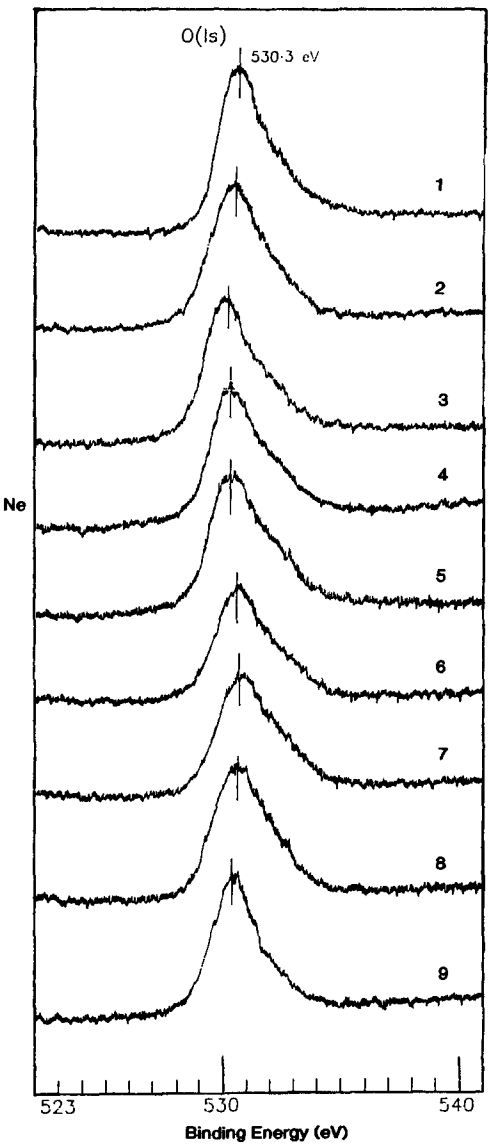

FIG. 13. XPS spectra recorded in the O (1*s*) region between various treatments for the CO hydrogenation study with potassium promoted Co/MnO. Spectra were recorded: (1) before treatment; (2) after 12 h H_2 (400°C); (3) after 15 min Fischer–Tropsch synthesis; (4) after 1 h Fischer–Tropsch synthesis; (5) after 3 h Fischer–Tropsch synthesis; (6) after 6 h Fischer–Tropsch synthesis; (7) after 12 h Fischer–Tropsch synthesis; (8) after 12 h H_2 (400°C); (9) after Ar^+ bombardment (5 kV beam energy for 5 min).

virtually unchanged during the Fischer–Tropsch treatments, indicating that the manganese at the surface remains in the form of MnO. The cobalt ($2p_{3/2}$) signal indicates that the oxide component at a BE of 780.5 eV increases, and this is highlighted by the appearance of a more prominent shake-up satellite.

The results from the present study show that an increase in the carbon (1*s*) signal with a BE of 285.1 eV is associated with an increase in the metallic component of the cobalt ($2p_{3/2}$) XPS signal, only after the catalyst surface has stabilized under Fischer–Tropsch conditions (ca 6 h).

The amount of carbon deposited during Fischer–Tropsch synthesis on the catalyst in the present study does not differ markedly with respect to unpromoted Co/MnO (*35*), although one would expect to see enhanced carbon buildup due to potassium promotion. A possible explanation is that the carbon observed at the surface is associated with metallic cobalt, and K_2CO_3 promotion of the Co/MnO catalyst inhibits reduction of the surface cobalt. This argument is further substantiated by reports of potassium delaying graphitization and carbon buildup on iron oxide surfaces (*38, 39*).

The catalyst was re-reduced after 12 h of Fischer–Tropsch synthesis, resulting in significant changes in the carbon (1*s*), potassium (2*p*), and cobalt (2*p*) XPS spectra. Re-reduction has the effect of removing most but not all of the surface carbon. There is still a carbon (1*s*) peak at a BE of 285.1 eV associated with carbon which has not been fully hydrogenated. Removal of a large portion of the carbon exposes the potassium as shown by the r.s.a.p. increase from 4.5 to 8.9% for potassium. Re-reduction of the catalyst has no effect on the Co/Mn ratio which is seen to remain unchanged at 0.32. The surface cobalt still mainly in the oxidized state as shown by the sharp cobalt ($2p_{3/2}$) signal at 779.7 eV which has a clear shake-up satellite indicating the presence of Co^{2+}. Re-reduction has no marked effect on the oxygen (1*s*) and manganese (2*p*) XPS signals.

Finally, a mild argon ion bombardment treatment was performed to ascertain the

TABLE 5

Mass/mass % of Hydrocarbon Components Detected for Various Times on Stream over K-Promoted Co/MnO Catalysts

Time on stream	Mass/mass % of hydrocarbon selectivity									
	C_1	$C_2=$	C_2	$C_3=$	C_3	C_4	C_5	C_6	MeOH	EtOH
15 min	40.5	2.6	6.3	5.5	3.3	10.9	15.3	15.6	tr	tr
1 h	34.3	2.3	6.3	7.2	3.6	20.6	6.7	18.9	—	—
3 h	84.3	0.5	9.9	0.5	2.2	1.8	0.5	0.4	—	—
6 h	40.7	3.8	5.3	7.9	2.6	19.0	8.3	12.5	—	—
12 h	62.4	0.7	14.5	2.1	8.1	5.1	3.0	4.1	—	—
15 min[a]	64.0	0.2	14.5	0.3	8.6	5.7	2.5	3.3	tr	tr
12 h[a]	66.0	0.1	11.6	0.1	7.3	4.5	1.7	4.9	—	—

[a] Ref. (*35*).

possible differences between the surface and the bulk catalyst. This treatment is shown to result in the removal of all the potassium, as is witnessed by the disappearance of the potassium ($2p$) signal. Removal of the potassium confirms that it segregates to the surface or near surface both before and during the various treatments. This corresponds with XRD findings which show that potassium promotion at the levels investigated here does not in any way affect the bulk structure of Co/MnO catalysts.

Apart from increases in the r.s.a.p.'s of oxygen and manganese, only the oxygen ($1s$) signal changes slightly after Ar^+ bombardment in that it is seen to become slightly narrower. This is presumably due to the removal of oxygen originating from K_2CO_3.

Furthermore, Ar^+ bombardment indicates that the subsurface cobalt is metallic as witnessed by the sharp cobalt ($2p_{3/2}$) peak at 778.3 eV and the disappearance of the shake-up satellite associated with Co^{2+} (as CoO). This reduced cobalt is associated with the removal of the potassium and gives credibility to the assumptions that reduction is initiated in the catalyst bulk and that the metallic cobalt is mobile. This is coupled to the idea that potassium inhibits reduction of cobalt at the surface.

The Role of the Potassium Promoter

Although it is well known that alkali promoters significantly modify the *catalytic activity* of metals for CO hydrogenation, there is disagreement in the literature on the specific mechanistic implications. For example, studies on silica-supported iron systems (*40*), carbon-supported iron–cobalt and carbonyl-cluster-derived catalysts (*31*), and Ru/TiO_2 catalysts (*41*) showed that potassium-promoted catalysts were less active than those catalysts without potassium. However, work by Arakawa and Bell (*17*) on alumina-supported iron catalysts and Dry (*6*) on fused catalysts operating at high temperatures in a fluidized bed showed increased activity with K_2O content. Interestingly, at low temperatures in a fixed bed, the activity decreased for the same fused catalysts as the K_2O content was increased.

Dent and Lin (*11*) have investigated the role of K promoters on supported Co/Mn catalysts. Their data indicate that the presence of K_2O results in an increase of C_2–C_4 olefin selectivity. Small amounts of K_2O

also resulted in lower methane production and higher wax production.

Our data show an initial increase in specific activity followed by a subsequent decrease in specific activity with increasing potassium content in the catalyst. We have also observed well-defined effects on the product selectivity. Thus, potassium-promoted catalysts give (i) lower methane selectivities, (ii) increased alkene/alkane ratios, and (iii) increased long-chain alcohol and alkane formation. The use of the combined characterization techniques enables us to suggest a possible explanation for these effects. The XPS data clearly indicate the migration of potassium to the catalyst surface during both the calcination and the CO-hydrogenation reactions. It is therefore clear that the potassium influences the surface and not the bulk catalyst properties (cf. XRD data).

The product selectivity suggests that the catalyst has become less hydrogenating and, by implication, that the C/H surface ratio has increased. Chemisorption studies on other Fischer–Tropsch catalysts have shown enhanced carbon and suppressed hydrogen coverage, which supports this suggestion (*12, 42, 43*). One proposal to rationalize this data involves the interaction of potassium with the CO. As potassium exists as the potassium ion in the catalyst (the Fischer–Tropsch reaction produces water), this explanation could entail reactions of the K^+ with the oxygen of the surface-bonded CO.

It also appears that the modification and decrease in activity is due to a change in the number of active catalyst sites. This would arise from (i) the presence of potassium on the surface, (ii) the presence of less-active CO on the surface (potassium can inhibit Co^{2+} to Co reduction), and hence less CO activation, or (iii) the presence of heavy hydrocarbons on the surface (*6*).

The XPS data support proposals (i) and (ii). It thus appears that potassium has two roles in our catalyst—to modify the concentration of cobalt active sites and to reduce the breakdown of the CO molecule.

CONCLUSION

For Co/MnO catalysts, maximum activity was obtained at a low potassium level and a small decrease in CO conversion was observed at the optimum potassium loadings of between 0.1 and 0.2% potassium. The alkali metal was observed to decrease the hydrogenation ability of the catalyst, as indicated by a decrease in methane selectivity and an increase in product (C_2 and C_3) olefinity. There was also an observed shift to higher-molecular-weight hydrocarbons with potassium promotion, a shift substantiated by increased chain-growth probability factors α calculated from Anderson–Schulz–Flory plots for the set of potassium-promoted catalysts. The presence of potassium also favored the formation of longer-chain alcohols, accompanied by decreases in selectivity toward the C_1OH–C_4OH fractions.

Selectivity of the C_2 and C_3 alkenes was studied as a function of reactor operating conditions. Increasing reaction temperature resulted in the catalyst's becoming increasingly hydrogenating while decreases in the olefinity of the C_2 and C_3 products were observed. Alkene selectivity was found to decrease with increasing reciprocal space velocity (space–time) and conversion and, at constant conversion, increasing pressure.

XRD and DSC characterization performed on the series of potassium-promoted catalysts suggested that the incorporation of the alkali did not in any way affect the bulk structure of the catalysts. The potassium promoter concentrated on the catalyst surface; changes in surface composition were demonstrated from BET surface area measurements and XPS studies. BET measurements showed the surface area to initially decrease at low levels and then to increase to levels consistent

with the unpromoted entry. XPS studies showed surface segregation of the potassium from the bulk to occur during calcination, reduction, and synthesis. They also showed a decrease in the number of surface Co sites as a result of diffusion limits set up within the MnO lattice.

APPENDIX (25)

Penn (*28*) has shown that relative surface concentrations of different atoms in an alloy, say for simplicity type 1 and type 2 atoms, can be given by the equation

$$\frac{\eta_1}{\eta_2} = \frac{I_1}{I_2}\frac{\sigma_2}{\sigma_1}\frac{D(\varepsilon_2)}{D(\varepsilon_1)}\frac{\lambda_T(\varepsilon_2)}{\lambda_T(\varepsilon_1)},$$

where η_1/η_2 is the relative concentration of type 1 and type 2 atoms, I_1/I_2 is the relative signal strength observed by XPS measurements, σ is the photoionization probability (as calculated by Schofield), D is the fraction of electrons detected by the analyzer, and $\lambda_T(\varepsilon_2)/\lambda_T(\varepsilon_1)$ is the ratio of the mean free paths of photoelectrons with energy ε_1 and ε_2 coming from type 1 and type 2 atoms in the alloy. This electron escape depth ratio can be shown to be approximated by the following equation:

$$\frac{\lambda_T(\varepsilon_2)}{\lambda_T(\varepsilon_1)} = \frac{(\varepsilon_2)}{(\varepsilon_1)}\{(\ln \varepsilon_1 - 2.3)/(\ln \varepsilon_2 - 2.3)\}.$$

This expression can be used directly in the first equation, which in turn can easily be modified to facilitate relative surface atomic percentage (herewith abbreviated as r.s.a.p.) calculations for more than two elements.

Furthermore, Penn states that to a fairly good approximation there is a material-independent behavior of $\lambda_T(\varepsilon_2)/\lambda_T(\varepsilon_1)$ as a function of ε_2 and ε_1 for $\varepsilon_1, \varepsilon_2 \geq 200$ eV. The use of the second equation for the calculation of photoelectron escape depths can be shown to result at most in an error of 14%, but more typically one in the region of 5% is incurred.

For the purpose of this study, relative atomic percentages of elements at the surface or near surface were calculated. These values were obtained using Penn's formulae as a basis.

In instruments where the analyzer energy is fixed, such as the one used in this study, the transmission is inversely proportional to the kinetic energy of the electrons, hence the Ds in the first equation can be replaced by values of $1/E_k$. Since the photoionization probability is directly proportional to the core level photoionization cross section (PIC) of an element, a PIC for each element can be substituted into the first equation as that element's σ value. A value of $\lambda_T(\varepsilon)$ for each element was calculated using the equation

$$\lambda_T(\varepsilon_1) = \frac{\varepsilon_1}{(\ln \varepsilon_1 - 2.3)},$$

where $\varepsilon_1 = E_k$ for photoelectrons from the element 1.

λ_T values calculated and used in the calculations were carbon (250.9), potassium (294.4), oxygen (210.0), manganese (190.3), and cobalt (166.0).

ACKNOWLEDGMENTS

We thank Drs. M. Dry and R. Espinoza of SASTECH, Sasolburg, for helpful discussions. We also thank the University, SASTECH, the National Energy Council, and the Foundation for Research and Development, Pretoria, for financial support.

REFERENCES

1. Shah, Y. T., and Perrotta, A. J., *Ind. Eng. Chem. Prod. Res. Dev.* **15,** 123 (1976).
2. Bussemeier, B., Frohning, C. D., and Cornils, B., *Hydrocarbon Process.* **55,** 105 (1976).
3. Storch, H. H., Golumbic, N., and Anderson, R. B., "The Fischer–Tropsch and Related Synthesis," Wiley, New York, 1951.
4. Flory, P. J., "Principles in Polymer Chemistry," Cornell Univ. Press, Ithaca, New York, 1967.
5. Anderson, R. B., "The Fischer–Tropsch Synthesis," Academic Press, Orlando, FL, 1984.
6. Dry, M. E., *in* "Catalysis—Science and Technology—Vol. 1" (J. R. Anderson and M. Boudart, Eds.), Chap. 4, p. 159, Springer-Verlag, Berlin, 1981.
7. Van der Lee, G., Bastein, G. T. M., van Boogert, I., Schuller, B., Luo, H. Y., and Ponec, V., *J. Chem. Soc. Faraday Trans.* **83,** 2013 (1987).

8. Gonzalez, R. D., and Miura, H., *J. Catal.* **77,** 338 (1982).
9. Anderson, R. B., "Catalysis—Vol. 4" (P. H. Emmett, Ed.), Von Nostrand–Reinhold, Princeton, NJ, 1956.
10. Dry, M. E., and Oosthuizen, G. J., *J. Catal.* **11,** 18 (1968).
11. Dent, A. L., and Lin, M., *in* "Advances in Chemistry Series," No. 178, p. 47, Amer. Chem. Soc., Washington, DC, 1979.
12. Dry, M. E., Shingles, T., Boshoff, L. J., and Oosthuizen, G. J., *J. Catal.* **15,** 190 (1969).
13. Konig, L., and Gaube, J., *Chem.—Eng.—Tech.* **55,** 14 (1983).
14. Van der Riet, M., Hutchings, G. J., and Copperthwaite, R. G., *J. Chem. Soc. Chem. Commun.*, 788 (1986).
15. Copperthwaite, R. G., Hutchings, G. J., van der Riet, M., and Woodhouse, J., *Ind. Eng. Chem. Res.* **26,** 869 (1987).
16. Van der Riet, M., Copperthwaite, R. G., and Hutchings, G. J., *J. Chem. Soc. Faraday Trans. 1* **83,** 2963 (1987).
17. Arakawa, H., and Bell, A. T., *Ind. Eng. Chem. Process Des. Dev.* **22,** 97 (1983).
18. Schulz, H., *C$_1$ Mol. Chem.* **1,** 231 (1985).
19. Varma, R. L., Dan-Chu, L., Mathews, J. F., and Bakhshi, N. N., *Can. J. Chem. Eng.* **63,** 72 (1985).
20. Courty, P., and Chaumette, P., *Energy Process* **7** (1), 23 (1987).
21. Colley, S. E., Copperthwaite, R. G., Hutchings, G. J., Terblanche, S. P., and Thackeray, M. M., *Nature* **339,** 129 (1989).
22. Maiti, G. C., Malessa, R., and Baerns, M., *Appl. Catal.* **5,** 151 (1983).
23. Acres, G. J. K., Bird, A. J., Jenkins, J. W., and King, F., "Catalysis—Specialist Periodical Reports—Vol. 4," Chap. 1, The Royal Society of Chemistry, London, 1981.
24. Copperthwaite, R. G., Loggenberg, P. M., Derry, T. E., and Sellschop, J. F. P., *Vacuum* **38,** 413 (1988).
25. Loggenberg, P. M., P.h.D. Thesis, University of the Witwatersrand, Johannesburg, South Africa, 1989.
26. Copperthwaite, R. G., Hack, H., Hutchings, G. J., and Sellschop, J. P. F., *Surf. Sci. Lett.* **164,** 827 (1985).
27. Roberts, M. W., and Smart, R. St. C., *Chem. Phys. Lett.* **69,** 234 (1980).
28. Penn, D. R., *J. Electron. Spectrosc. Relat. Phenom.* **8,** 29 (1976).
29. Yang, G. H., and Oblad, A. G., *Prepr. Am. Chem. Soc. Div. Pet. Chem.* **23** (2), 513 (1978).
30. Bukur, D. B., Mukesh, D., and Patel, S. A., *Ind. Eng. Chem. Res.* **29,** 194 (1990).
31. Chen, A. A., Kaminsky, M., Geoffroy, G. C., and Vannice, M. A., *J. Phys. Chem.* **90,** 4810 (1986).
32. Colley, S. E., Copperthwaite, R. G., and Hutchings, G. J., *Catal. Today* **9,** 203 (1991).
33. Themistocleous, T., University of the Witwatersrand, personal communication (1989).
34. Wesner, D. A., Linden, G., and Bonzel, H. P., *Appl. Surf. Sci.* **26,** 335 (1986).
35. Betts, M. J., Masters Dissertation, University of the Witwatersrand, Johannesburg, South Africa (1989).
36. Bonzel, H. P., Broden, G., and Krebs, H. J., *Appl. Surf. Sci.* **16,** 373 (1983).
37. Grzybek, T., Papp, H., and Baerns, M., *Appl. Catal.* **29,** 351 (1987).
38. Somorjai, G. A., *Surf. Sci.* **89,** 496 (1979).
39. Somorjai, G. A., *Catal. Rev. Sci. Eng.* **23,** 189 (1981).
40. Yeh, E. B., Schwarts, L. H., and Butt, J. B., *J. Catal.* **91,** 241 (1985).
41. Chuang, S. C., Goodwin, J. G., Jr., and Wender, I., *J. Catal.* **95,** 435 (1985).
42. Ertl, G., Lee, S. B., and Weiss, M., *Surf. Sci.* **111,** L711 (1981).
43. Koel, B. E., Peebles, D. E., and White, J. M., *Surf. Sci.* **107,** 367 (1981).